Int. J. Heat Mass Transfer. Vol. 15, pp. 127–145. Pergamon Press 1972. Printed in Great Britain

STRUCTURE OF TURBULENT VELOCITY AND TEMPERATURE FIELDS IN ETHYLENE GLYCOL PIPE FLOW AT LOW REYNOLDS NUMBER

ASHOK K. KUDVA* and ALEXANDER SESONSKE
Department of Nuclear Engineering, Purdue University, Lafayette, Indiana 47907, U.S.A.

(*Received* 30 *March* 1971)

Abstract—Mean velocity profiles and turbulent intensities under isothermal conditions were measured in ethylene glycol flowing through a 1·434 in. i.d. vertical pipe at a Reynolds number of about 6000. In addition, the rms temperature fluctuation t' and the turbulent velocity–temperature correlation $\overline{u_x t}$ were also measured under a uniform heat flux of 8000 Btu/hft^2, using a hot-film sensor. Temperature spectra at various radial locations, the velocity spectrum at the center of the pipe and various scales of turbulence were estimated.

Results show that the mean velocity distribution in the turbulent core lies above the "universal velocity profile." Comparison with Laufer's data indicates that the structure of isothermal turbulence within the viscous sublayer is independent of Reynolds number within the range N_{Re} = 6000–50 000. Near the center of the pipe u_x' and t' exhibit radial homogeneity. In this region, the turbulent velocity–temperature field approaches isotropy. The velocity spectra estimated do not exhibit a wave number region with a $-\frac{5}{3}$ slope as predicted by Kolmogoroff, nor do the temperature spectra follow the predictions of Batchelor's uniform straining model under the low N_{Re}, high N_{Pr} conditions of the experiment.

NOMENCLATURE

C_p, specific heat at constant pressure;
e, instantaneous voltage fluctuation;
e', root-mean-square voltage fluctuation;
E, instantaneous bridge voltage;
$\bar{E}$, time averaged d.c. voltage;
E_t, spectrum function of the temperature fluctuation, t; Reynolds number;
E_u, three dimensional spectrum function of the velocity fluctuation, u;
E_{1u}, one dimensional spectrum function;
E_{1ut}, one dimensional spectrum of $\overline{u_x t}$;
f, frequency [Hz];
f, friction factor;
k, wave number, $2\pi f/\bar{U}$;
N_{Re}, Reynolds number, subscript f indicates physical properties evaluated at the film temperature;
N_{Pr}, Prandtl number, subscript f indicates physical properties evaluated at the film temperature;
P, pressure;
q_w, heat flux at the wall;
R, radius of the pipe;
R_a, resistance of the sensor at ambient temperature;
R_s, resistance of the sensor at operation temperature;
R_λ, turbulent Reynolds number;
r, distance from the center of the pipe;
S_u, velocity sensitivity of the hot film sensor;
S_t, temperature sensitivity of the hot film sensor;
T, instantaneous temperature;
$\bar{T}$, time averaged temperature;
T^*, friction temperature, $q_w/\rho C_p U^*$;

* Present address: E. I. duPont de Nemours & Co., Photo Products Department, Parlin, New Jersey 08859.

$\overline{T}_w$, wall temperature, time averaged;
T_s, sensor temperature;
T^+, $(T_w - \overline{T})/T^*$;
t, fluctuating component of temperature;
t', root-mean-square temperature fluctuation;
U, instantaneous velocity [ft/s];
$\overline{U}$, time averaged velocity;
u_x, u_r, instantaneous velocity fluctuations in the axial and radial directions, respectively;
u'_x, rms velocity fluctuation in the axial direction;
$\overline{u_x u_r}$, Reynolds stress component;
$\overline{u_x t}$, axial-velocity–temperature correlation;
U^* friction velocity;
U^+, $\overline{U}/U^*$;
y, distance from the pipe wall;
y^+, $U^* y/\nu$;
α, rate of change of sensor resistance with temperature;
∂, partial differential operator;
δ thickness of the viscous sublayer;
δ_T, thickness of the thermal sublayer;
ε_u, rate of dissipation of the kinetic energy of turbulence per unit mass;
ε_t, rate of dissipation of the 'energy' of temperature fluctuations per unit mass;
Λ_x, Eulerian integral scale or macroscale of velocity fluctuations;
Λ_t, integral scale of temperature fluctuations;
λ_x, microscale of velocity fluctuations;
λ_t, microscale of temperature fluctuations;
μ, viscosity;
ρ, density;
ν, kinematic viscosity;
σ, thermal diffusivity;

INTRODUCTION

Background

THIS investigation is part of a larger program concerned with turbulence characteristics of several fluids covering a range of Prandtl number and at a range of Reynolds numbers in order to achieve a better understanding of turbulent transport phenomena.

From experimental data for turbulent flow in circular pipes, several empirical expressions have been formulated in the literature to describe the mean velocity profile and friction factor. Such empirical versions of a "universal velocity profile," or "law of the wall" give reasonably good predictions of these parameters for Reynolds numbers above 30000. A recent work by Reynolds [1], however, indicated that in the Reynolds number range of 5000–30000, even the friction factors deviate from the empirical predictions by more than 20 per cent.

For the higher Reynolds numbers, we have the detailed measurements by Laufer [2] made in air flowing through a pipe at Reynolds numbers of 50000 and 500000. The results of Patterson [3] and Knox [4] for organic liquids flowing in pipes agree with Laufer's results at nearly the same Reynolds numbers. However, with the exception of the measurements of Bakewell [5] in glycerine at $N_{Re} = 8700$, few measurements in liquids or even in air are reported for turbulent pipe flow at low Reynolds numbers.

Several sets of experimental data for rms intensities of turbulent temperature fluctuations in fluids flowing through pipes have also been reported in the literature, eg for air by Tanimoto and Hanratty [6], for water by Subbotin *et al.* [7], for mercury by Bobkov *et al.* [8] and for both mercury and ethylene glycol by Rust and Sesonske [9]. Extension of these measurements to turbulent velocity temperature correlations, which represent the heat flux transported by turbulence is desirable for understanding the nature of such transport. The axial turbulent velocity-temperature correlation $\overline{u_x t}$ has been measured for air in thermal boundary layers by Johnson [10] and Arya [11]. However, no measurements for pipe flow have been reported.

The theoretical models

A one dimensional spectrum $E_{1u}(k)$ of the velocity fluctuation u_x can be defined so that

$$\overline{u_x^2} = \int_0^\infty E_{1u}(k)\,\mathrm{d}k \tag{1}$$

where k is the wave number related to both the frequency f, and the mean velocity $\overline{U}$, by the relation

$$k = \frac{2\pi f}{\overline{U}}. \tag{2}$$

A three dimensional spectrum function $E_u(k)$ is more convenient than $E_{1u}(k)$ for theoretical treatments. In an isotropic turbulent field, if $E_{1u}(k)$ varied as k^n, it can be shown that $E_u(k)$ also varies as k^n. Experimentally measured one dimensional spectra can, therefore, be used to test the validity of various spectral theories.

The theories of Kolmogoroff [12], Heisenberg [13], Pao [14] and Kraichnan [15] predict the shape of the three dimensional spectrum. According to Kolmogoroff's hypotheses, at large Reynolds numbers the small scale components of motion become isotropic and independent of large scale motion. Also, there develops a wave number region in which the transfer of energy among different scales of motion will be governed by inertial transfer. In this inertial subrange, $E_u(k)$ is independent of the kinematic viscosity ν, and varies with k as

$$E_u(k) = C\varepsilon_u^{\frac{2}{3}}k^{-\frac{5}{3}} \tag{3}$$

where ε_u is the rate of dissipation of turbulent energy per unit mass and C is a constant.

At very large values of k, where viscosity plays an important role, $E_u(k)$ varies as k^{-7}, according to Heisenberg, so that

$$E_u(k) = C_1\varepsilon_u^{\frac{2}{3}}\nu^{-4}k^{-7}. \tag{4}$$

Spectra of velocity fluctuation measured by Laufer [2] show a $-\frac{5}{3}$ region for the turbulent Reynolds number $R_\lambda < 200$, when the mean velocity gradients were not too large. On the other hand, the Heisenberg theory has not been adequately tested experimentally. In fact there are little data available to validate either theory for low Reynolds number pipe flow.

The problem of turbulent scalar mixing was developed by Obukhov [16] and Corrsin [17] along the lines of the theory of Kolmogoroff for turbulent motion. They showed that the spectrum $E_t(k)$ of the scalar fluctuation t, would have a convective subrange with a spectral form

$$E_t(k) = A\varepsilon_u\varepsilon_t^{-\frac{1}{2}}k^{-\frac{5}{3}} \tag{5}$$

where A is a dimensionless constant ε_u and ε_t are the dissipation rates of the velocity and temperature fluctuations and k is the wave number. Batchelor [18] pointed out that for fluid systems with large Prandtl numbers a viscous–convective subrange would exist beyond this convective subrange. From a uniform straining model, he showed that in the viscous–convective subrange the spectrum would vary as k^{-1}. Beyond this viscous convective subrange, a viscous–diffusive subrange would exist in which a rapid decay would occur.

Concentration and temperature spectra measured in a water tunnel by Gibson and Schwartz [19] and concentration spectra measured in a pipe by Nye and Brodkey [20] are in agreement with Batchelor's uniform straining model. However, this model has not received experimental support when applied to turbulent temperature fields in high Prandtl number fluids flowing through pipes.

Objectives

This work was undertaken to investigate the structure of turbulence in pipe flow at the relatively unexplored low Reynolds number of 6000, in both isothermal as well as nonisothermal conditions (under a uniform heat flux of 8000 Btu/h ft^2). Specifically, (1) to compare the mean velocity profile obtained with the others available for approximately the same Reynolds number, as well as with the "universal velocity profile" prediction, (2) to compare the intensities of axial velocity fluctuations obtained at this low Reynolds number with those reported by Laufer at higher Reynolds numbers of 50000

and 500000, (3) to compare all the above isothermal features with the corresponding results obtained for the nonisothermal case, (4) to obtain the radial distribution $\overline{u_x t}$, representing the heat flux transported in the axial direction by turbulence, which hitherto has not been reported for pipe flow, (5) to obtain the spectrum of $\overline{u_x t}$ which also has not been reported to date and, (6) to compare the measured velocity and temperature spectra with the theoretical predictions.

EXPERIMENTAL DETAILS

Apparatus

As shown in Fig. 1, the fluid studied, ethylene glycol was circulated through a test section in a primary loop by a 15 h.p. canned stainless steel pump, with heat removal available through heat exchange to fluids in a secondary system. A Cunofilter, with a 5 μ nominal and 25 μ absolute rating installed in the discharge side of the pump ensured clean liquid in the loop, an essential requirement for hot film anemometry.

The primary loop consisted of a test section of contour-welded and honed $1\frac{1}{4}$-in. schedule-10 stainless steel pipe with a test section 16 ft long, corresponding to a L/D ratio of 132. For the nonisothermal runs, the last 67 diameter length of the test section was electrically heated using $\frac{3}{16}$ in. $\times$ 0·0178 in. Nichrome ribbon wound in grooves cut in a $\frac{1}{8}$-in. thick layer of Sauereisen cement covering the pipe. Insulation of the test section was provided by successive layers of asbestos string, asbestos and fiber glass.

Another pipe section designed to be hydraulically identical to the test section, with an equal L/D ratio, was used for the return line and provided with four static pressure taps at one-foot intervals for pressure drop measurements.

Instruments

A hot film sensor, a total head tube and pitot-static tube were positioned in the test section by means of a micrometer-driven traversing mechanism. The radial location of each probe could be determined to an accuracy of 0·001 in. with a backlash error of 0·002 in.

The total-head tube of a "fish-mouth" design had a bore of 0·008 in. $\times$ 0·023 in., with the smaller side parallel to the direction of traverse. Static pressure was determined by a pitot-static tube, kept at a fixed location. Pressures from these two sources were transmitted to the two sides of a calibrated Pace Model P-7 Variable Reluctance Transducer to measure mean velocities.

Two pressure taps from the return section were connected to the two sides of a calibrated Foxboro Model 613 DL D.P. Cell to measure pressure gradient.

A hot film probe, specially made by Thermo Systems, Inc. was used to obtain turbulence characteristics. This probe consisted of a 1000 Å thick and 0·020 in. long platinum film and a 0·001 in. dia. quartz rod. A thin coating of gold maintained electrical contact between the sensor support and the film. The platinum film was coated with a 16000 Å thick layer of sputtered quartz. The gold coating and the support needles were coated with a silicone compound to isolate them electrically from ethylene glycol. A series of compounds was tried for this purpose before arriving at a suitable material sufficiently resistant to the corrosive action of ethylene glycol.

Iron–constantan thermocouples were used to measure all time-averaged temperatures with thermoelectric voltages relative to an ice junction amplified by a Dana Model 2854 Differential Amplifier at a gain of 1000. A traversing 0·015-in. diameter chromel–constantan thermocouple was used to measure the radial distribution of the mean temperature during the nonisothermal runs. Thermocouples were also installed in the mixing chambers on both sides of the test section and along the wall of the test section as indicated in Fig. 1.

Electronic instrumentation

Figure 2 shows the instrumentation arrangement used to obtain the turbulence data. With a

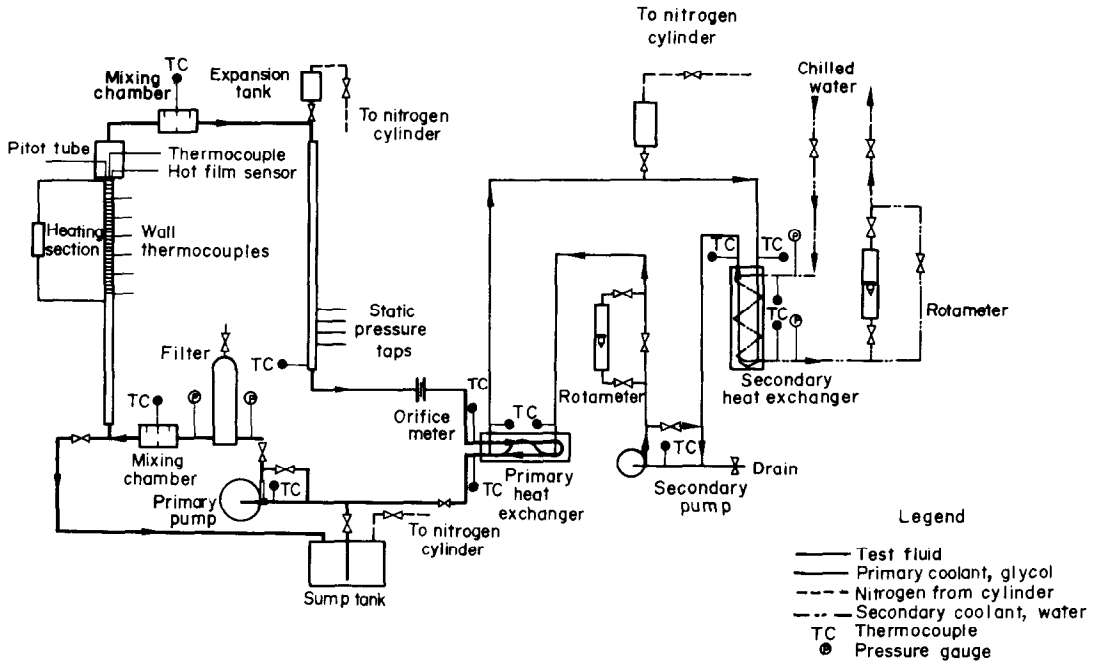

FIG. 1. Heat transfer loop.

TSI Model 1040 Temperature and Switching Circuit connected to the hot-film sensor in the Velocity Mode, the anemometer unit was operated as a constant temperature anemometer. In the d.c. 1000 Hz band width, output noise of the anemometer unit was less than 0·002 per cent equivalent turbulent intensity according to the manufacturer's specifications. A TSI Model

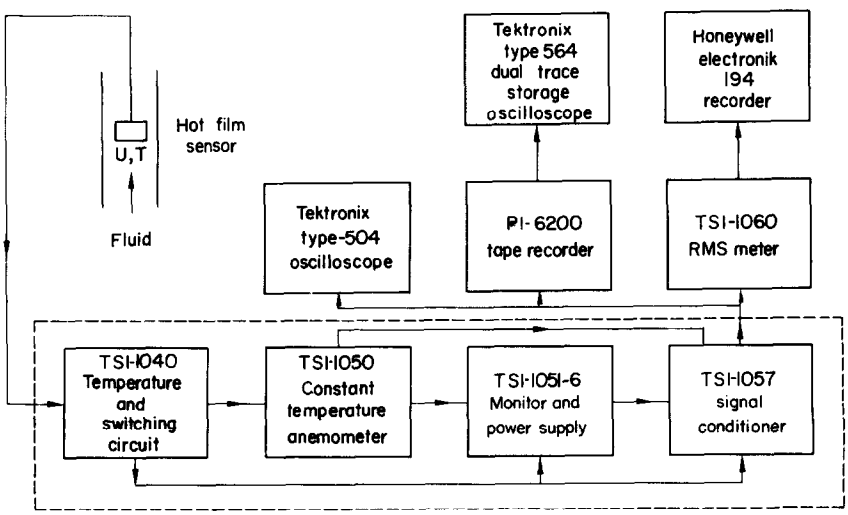

FIG. 2. Instrumentation for data acquisition.

1057 Signal Conditoner, with a flat frequency response from d.c. to 40000 Hz was used to amplify the low level turbulence signal near the center of the pipe by a gain of 10 to facilitate recording. A 4-channel, Precision Instrument Company, Model PI-6200 Tape Recorder with a flat frequency response from d.c. to 100, 1 kHz, and 10 kHz at 1 dB attenuation points at recording speeds of 0·375, 3·75 and 37·5 i.p.s., respectively, was used to record the signal. Root-mean-square intensities were measured using a TSI Model 1060 RMS Volt Meter, which has a 1 dB attenuation at 0·1 and 0·3 Hz at time constants of 100 and 30 s, respectively.

A General Radio Type 1564-A Sound and Vibration Analyzer, with a constant per cent bandwidth of 7 per cent in the range of 2·5 Hz to 25000 Hz was employed to perform a frequency analysis of the recorded signal.

Additional details of the experimental apparatus and instrumentation are given by Kudva [21].

DATA AQUISITION

Isothermal mean velocity profile

Mean velocities were obtained in duplicate at 31 different points between the center and the wall of the pipe. Near the wall, the Reynolds numbers based on the impact tube radius were quite small. Since, under such conditions, the measured impact pressures differ from the true total pressures as a result of viscous effects, impact tube coefficients as given by Hurd, Chesky and Shapiro [22] were used to correct the measurements. The magnitude of the correction was greater than 3 per cent for only the three points closest to the wall, the maximum correction being 8 per cent.

Isothermal turbulent intensities

The resistance of the hot-film sensor, at a given temperature in glycol, increased gradually with time. However, the calibration data were reproducible at a given value of $R_s - R_a$, where R_s and R_a are the resistances of the sensor at the operating and the ambient temperatures, respectively. The intensity of turbulence at each location was measured by operating the sensor with at least two different values of $R_s - R_a$. The sensor was calibrated at a given value of $R_s - R_a$ by noting the anemometer d.c. voltage, E, at different values of the mean velocity, $\bar{U}$ at the center of the pipe. The calibration data in ethylene glycol at a given value of $R_s - R_a$ could be described using two constants A and B as

$$\bar{E}^2 = A + B\bar{U}^{0.45} \tag{6}$$

Turbulent intensity, u'_x, was obtained from the rms voltage, e', as

$$u'_x = e' \Big/ \frac{\partial \bar{E}}{\partial \bar{U}}. \tag{7}$$

From the scatter in the calibration data about the regression line, standard errors in the turbulent intensities were estimated. These varied from ± 20 per cent at the center of the pipe to ± 50 per cent near the wall. However, the difference between the intensities measured at two different values of $R_s - R_a$ was much smaller. This difference was negligible near the center and equal to 16 per cent near the wall of the pipe.

Isothermal spectra

To perform a frequency analysis, a 20 ft length of the recorded signal was played back as an endless tape loop at a speed of 3·75 i.p.s. with output signal passed through the wave analyzer. Spectra in the range of 0·25–1000 Hz were obtained using the signal recorded at speeds of 0·375 and 3·75 i.p.s.

Due to the finite length of the recorded signal, the measured spectral estimates have a 90 per cent confidence limit of ± 18 per cent above 2·5 Hz and below this frequency the maximum uncertainty is ± 65 per cent at 0·25 Hz. The errors in the measured spectra due to the finite length of the sensor were estimated to be less than 5 per cent at wave numbers below 1000 ft^{-1}. These calculations are described by Kudva [21].

From the spectral data, the Eulerian integral scale or macroscale Λ_x and the microscale λ_x were computed using the relations

$$\Lambda_x = \frac{\pi}{2\bar{u}_x^2} \lim_{k \to 0} E_{1u}(k) \tag{8}$$

and

$$\frac{2}{\lambda_x^2} = \frac{1}{2\bar{u}^2} \int_0^\infty k^2 E_{1u}(k)\, dk. \tag{9}$$

MEAN VELOCITY PROFILE

Nonisothermal measurements

All isothermal data were obtained with the Reynolds number at bulk temperature conditions equal to 6032 and with a constant wall heat flux of 8000 Btu/h ft^2.

Mean velocities were obtained at 33 different locations between the wall and the center of the pipe. The friction velocity U^* was estimated using the friction factor determined from the Blasius equation with the physical properties evaluated at the film temperature (average between wall and bulk temperatures).

From the mean velocity profile data, the dimensionless turbulent shear stress $\overline{u_x u_r}/U^{*2}$ was estimated using the relation

$$\frac{\overline{u_x u_r}}{U^{*2}} = \frac{r}{R} - \frac{\nu}{U^{*2}} \frac{d\bar{U}}{dr} \tag{10}$$

where ν is the kinematic viscosity, r is the distance from the wall, R is the radius of the pipe, u_x and u_r are the fluctuating velocities in the axial and radial directions and U is the instantaneous velocity in the axial direction. The bar indicates a time average.

Nonisothermal mean temperature profile

Mean temperatures were measured in duplicate at 24 different locations between the center and the wall. An indication of the consistency of the measurements is provided by a heat balance in which the sensible heat change of 23 700 Btu/h determined from flow rate and temperature measurements compared with an electrical input of 25 000 Btu/h.

Turbulence quantities, t', u', $\overline{u_x t}$

With the hot film sensor operated as a calibrated resistance thermometer, root mean square temperature fluctuations t' were obtained from the rms voltage. In this mode, the sensor had a flat frequency response up to a 3 db attenuation at 460 Hz and had negligible sensitivity to velocity changes, as shown by Kudva [21].

The hot-film sensor, when operated as a constant temperature anemometer, at a temperature of T_s responds to the mean temperature $\bar{T}$ and the mean velocity $\bar{U}$ with a d.c. voltage $\bar{E}$ as

$$\bar{E}^2 = (a + b\bar{U}^n)\,\alpha(R_s - \bar{R}) \tag{11}$$

where R_s and R are the sensor resistances at temperatures T_s and $\bar{T}$, α is the rate of change of the sensor resistance with temperature, and a and b are experimentally determined constants with $n = 0{\cdot}45$.

The sensor response e to instantaneous fluctuations in the fluid temperature t, and the the velocity u_x can be described by

$$e = S_u u_x - S_t t. \tag{12}$$

where

$$S_u = \frac{\partial \bar{E}}{\partial \bar{U}} \quad \text{and} \quad S_t = -\frac{\partial \bar{E}}{\partial \bar{T}}.$$

Upon squaring and time averaging, equation (12) becomes

$$\bar{e}^2 = S_u^2 \bar{u}_x^2 - 2S_u S_t \overline{u_x t} + S_t^2 \bar{t}^2. \tag{13}$$

Let

$$Y = \frac{\bar{e}^2}{S_t^2},\ X = S_u/S_t,\ A = \overline{u_x^2},\ B = -2\overline{u_x t}$$

then equation (13) becomes

$$Y = AX^2 + BX. \tag{14}$$

By fitting equation (14) to the fluctuation data obtained by operating the sensor at 9 different values of $R_s - R_a$, $\overline{u_x t}$ and u_x' were obtained

from the slope at the origin and the curvature of the parabola given by equation (14) as suggested by Arya [11]. Since only two operating values of $R_s - R_a$ were needed to determine u'_x and $\overline{u_x t}$, but nine were actually used the standard error in the expected value of u'_x and $\overline{u_x t}$ could be determined with seven degrees of freedom. A polynomial regression technique was used to fit equation (14) to the fluctuation data to obtain the values of u'_x and $\overline{u_x t}$ and the standard errors.

Spectra and scales of turbulence

Random signal output from the resistance thermometer representing temperature fluctuations was recorded and the spectral analysis was performed in the range of 0·25–1000 Hz. The signal from the resistance thermometer in the absence of temperature fluctuations representing noise was also taped and analyzed.

Random signals from the constant temperature hot-film anemometer at eight different values of $R_s - R_a$ at each radial location were recorded and analyzed in order to obtain the spectra of u'_x and $\overline{u_x t}$. The spectrum of the random signal output of the constant temperature hot-film anemometer is related to the spectra of $\overline{ut}$, u' and t' by the relation

$$E(f) = S_u^2 E_{1u}(f) - 2S_u S_t E_{1ut}(f) + S_t^2 E_{1t}(f) \qquad (15)$$

where E_{1u}, E_{1ut} denote the one dimensional spectra of u'_x, $\overline{u_x t}$ and t', respectively. Although it seemed possible to estimate the spectra of u'_x and $\overline{u_x t}$, computations resulted in inconsistent values of E_{1u} and E_{1ut}. In fact, at most frequencies, the values of E_{1u} obtained were negative. This is attributed to uncertainties in the measured spectra of the random signal.

Near the center of the pipe, the $\overline{u_x t}$ contribution was negligible and it was reasonable to assume that E_{1ut} is negligible compared with the spectra of u'_x and $\overline{u_x t}$. With this assumption, the spectrum of u'_x near the center of the pipe was estimated as

$$E_{1u}(f) = \frac{E(f) - S_t^2 E_{1t}(f)}{S_u^2}. \qquad (16)$$

The microscale λ_t and the macroscale Λ_t of the temperature fluctuations were calculated using the equations

$$\frac{2}{\lambda_t^2} = \frac{1}{\overline{t^2}} \int_0^\infty k^2 E_{1t}(k)\, dk \qquad (17)$$

$$\Lambda_t = \frac{\pi}{2\overline{t^2}} \lim_{k \to 0} E_{1t}(k). \qquad (18)$$

where $E_{1t}(k)$ is the measured one dimensional temperature spectrum. Since the spectral data in the low wave number region were scattered and the function $k^2 E_{1t}(k)$ had to be linearly extrapolated to evaluate the integral term in equation (17), the values of the scales obtained should be considered order of magnitude estimates.

RESULTS

The mean velocity profiles, temperature profiles, axial turbulence intensities and the axial spectra are presented here in graphical form. Tabulations of these are given by Kudva [21].

Mean velocity profiles

Figure 3 shows for the isothermal case the magnitude of the viscous effect correction with both corrected and uncorrected velocities indicated as fractions of the center line velocity $\overline{U}_{max}$. Only the data close to the wall of the pipe are shown. The slope of the mean velocity profile at the wall can be estimated from the pressure drop data as

$$\left[\frac{d\overline{U}_{max}}{dy/R}\right]_{y=0} = \frac{R}{2}\frac{dP}{dx}\frac{1}{\mu}\frac{R}{\overline{U}_{max}} \qquad (19)$$

where μ is the fluid viscosity, dP/dx is the pressure drop per unit length of the pipe, y is the distance from the wall and R is the pipe radius. Pressure drop can also be predicted

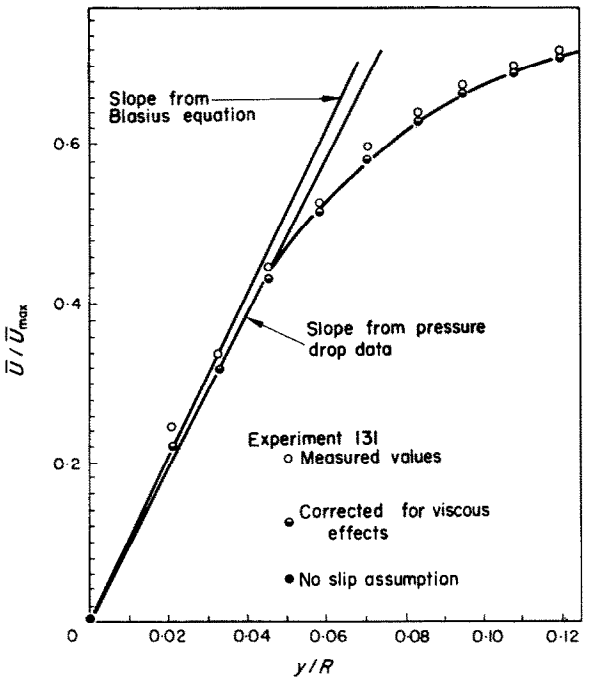

FIG. 3. Viscous effects on the mean velocity measurements.

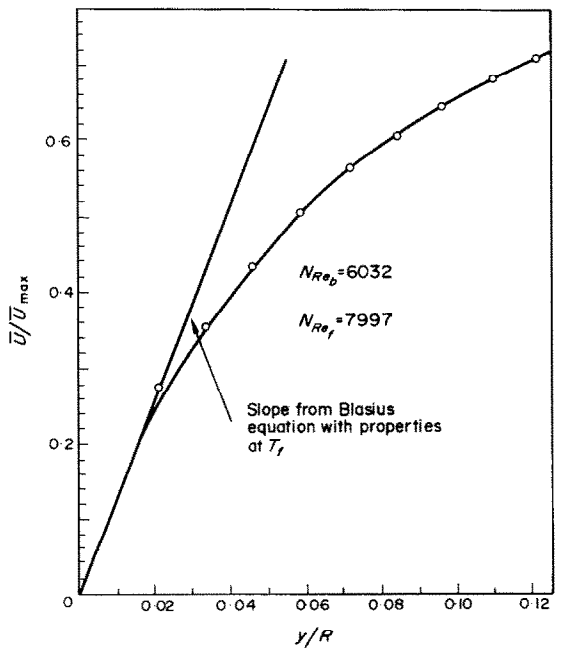

FIG. 4. Nonisothermal mean velocity profile near the wall.

using the friction factor f from the Blasius equation,

$$f = \frac{0{\cdot}079}{N_{Re}^{0{\cdot}25}}. \tag{20}$$

The slopes of the mean velocity profile at the wall estimated from pressure drop measurements and also from the Blasius equation are shown in Fig. 3.

The corrected mean velocity profile and the measured pressure drop are compatible with each other, but the Blasius equation overpredicts the measured pressure drop by 8 per cent, as shown in Fig. 3.

Figure 4 shows the same data for the nonisothermal condition. Since pressure drop data could not be obtained, the similarity parameter U^* was determined from the Blasius equation for friction factor.

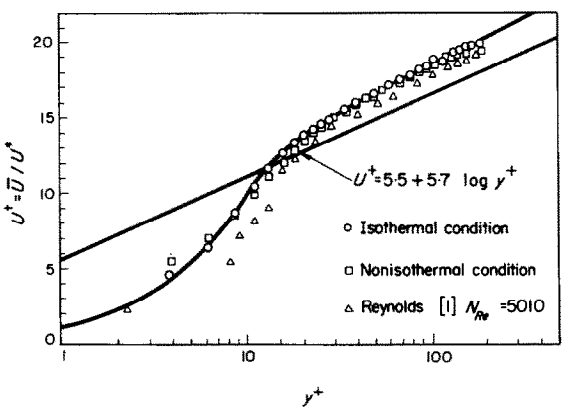

FIG. 5. Mean velocity distribution plot.

In Fig. 5, the mean velocity data for both cases are plotted in generalized coordinates, $U^+ = U/U^*$ against $y^+ = yU^*/\nu$, where ν and U^* are the kinematic viscosity and friction velocity, respectively. In evaluating y^+ for the nonisothermal case, the kinematic viscosity was estimated at the local fluid temperature. As a basis for comparison, the data obtained by Reynolds [1] in air flowing through a pipe at $N_{Re} = 5010$ are also shown in Fig. 5.

For y^+ less than 10, the present data fall along the curve for the viscous sublayer $U^+ = y^+$. In the turbulent core, the present data lie above the mean velocity distribution predicted by the "Universal Velocity Profile," $U^+ = 5{\cdot}5 + 5{\cdot}7 \log y^+$. Both the isothermal and nonisothermal profiles agree among themselves and also with the data of Reynolds. They are also in agreement with the data of Patel and Head [23]. This tends to the conclusion that at low Reynolds numbers, in the turbulent core, the "Universal Velocity Distribution" predicts values that are low.

Mean temperature distribution

Figure 6 shows the radial distribution of the dimensionless mean temperature

$$T^+ = \frac{\bar{T}_w - \bar{T},}{T^*}$$

where $\bar{T}_w$ is the wall temperature and T^* is defined by

$$T^* = \frac{q_w}{\rho C_p U^*} \tag{21}$$

where q_w is the heat flux at the wall and ρ and C_p are the density and the specific heat of the

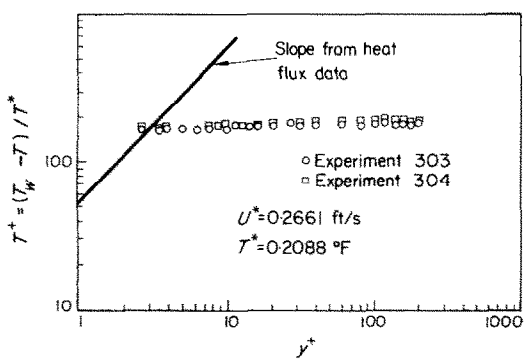

FIG. 6. Generalized mean temperature distribution.

fluid, respectively. In this type of plot, the mean temperature profile within the thermal sublayer can be represented by a straight line of unit slope with an intercept equal to the Prandtl number evaluated at the film temperature, N_{Prf}, as shown by Kudva [21]. The y^+ coordinates were evaluated at the bulk temperature T, which was almost equal to the local temperature, except for two points closest to the wall for which the film temperature was used in order to provide a more consistent temperature distribution pattern.

It is seen from Fig. 6 that the bulk of the resistance to thermal transport occurs within the thermal sublayer, the thickness of which is taken as the distance from the wall corresponding to the intersection of the mean temperature profile measurements and the thermal sublayer profile estimated from the heat flux data. In Fig. 6, this distance corresponds to $y^+ = 2{\cdot}5$. From Fig. 5, it is seen that the mean velocity profile deviates from the viscous sublayer curve, $U^+ = y^+$ at roughly $y^+ = 10$. The ratio of the thickness of the thermal sublayer δ_T to the thickness of the viscous sublayer δ, is then given by

$$\frac{\delta_T}{\delta} = \frac{2{\cdot}5}{10} = \frac{1}{4}. \tag{22}$$

For heat transfer in a laminar boundary layer over a flat plate, a theoretical expression for the ratio of the thicknesses of the thermal and viscous sublayer is given by Eckert and Drake [24] as

$$\frac{\delta_T}{\delta} = \frac{1}{1{\cdot}026\, N_{Pr}^{\frac{1}{3}}}. \tag{23}$$

Using equation (23) at $N_{Pr_f} = 53$, a value of 1/3·83 is obtained for δ_T/δ, which is approximately equal to the value of δ_T/δ determined experimentally.

Since the thickness of the thermal sublayer, corresponding to $y^+ = 2{\cdot}5$, is 0·006 in., while the diameter of the traversing thermocouple junction was 0·015 in., it was not possible to experimentally determine the temperature profile within the thermal sublayer.

Turbulent velocity intensities

The radial distribution of the root-mean-

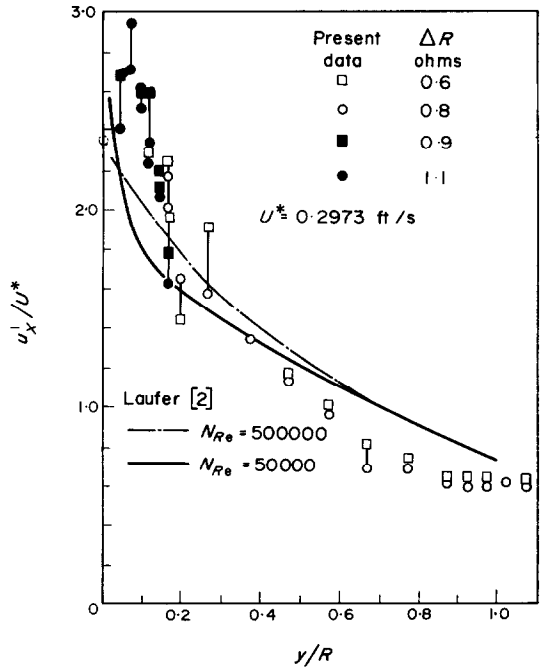

FIG. 7. Isothermal turbulent intensities (y/R plot).

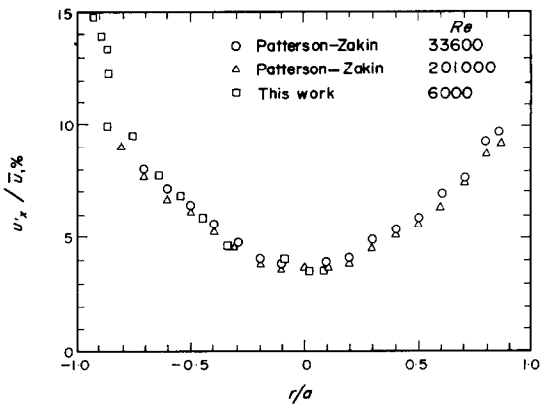

FIG. 9. Comparison of turbulence intensity profiles for toluene and ethylene glycol.

square turbulent intensity u'_x, relative to the friction velocity U^* measured in ethylene glycol at $N_{Re} = 5980$, under isothermal conditions, is presented as a function of y/R in Fig. 7 and y^+ in Fig. 8. For comparison, the distribution of u'_u/U^* measured in air at $N_{Re} = 50000$ and 500000 by Laufer [2] are also shown in the same figures. In Fig. 9 some of the present data (as $u'_x/\bar{U}$) are compared with the published results of Patterson and Zakin [25] for toluene at higher Reynolds numbers and seem to agree very well.

As seen from Fig. 7, between $y/R = 0{\cdot}89$ and the center of the pipe, the measured values of u'_x change little with radial location. The measured axial turbulent velocity field, therefore approaches radial homogeneity in this region.

Laufer's data indicate that near the center of the pipe, u'_x/U^* seems to be independent of Reynolds number. The present data in ethylene glycol at $N_{Re} = 5980$ give u'_x/U^* values near

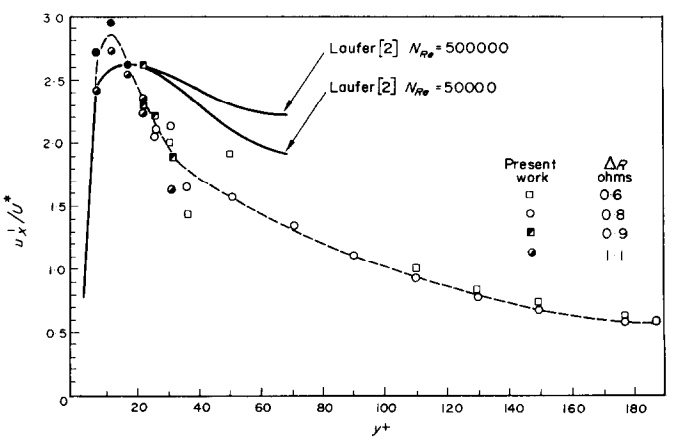

FIG. 8. Isothermal turbulent intensities (y^+ plot).

the center of the pipe approximately 20 per cent less than those reported by Laufer in air at higher Reynolds numbers. However, the uncertainty of intensity measurements itself is about 20 per cent.

The present data indicate that u'_x/U^* reaches a maximum between $y^+ = 10$ and $y^+ = 15$. Laufer's data also exhibit this behavior, as seen in Fig. 8. The maximum value of u'_x/U^* measured exceeds the corresponding values measured by Laufer by 7 per cent. This again may well be due to the random errors in the present data, rather than a Reynolds number effect.

From the radial distribution of the turbulent energy production and dissipation terms, Laufer concluded that (1) the bulk of the direct viscous dissipation takes place in a narrow region adjacent to the wall, $y^+ < 15$, and (2) the maximum amount of turbulent energy is produced at the edge of the viscous sublayer at $y^+ = 11{\cdot}5$. The maximum value of u'_x measured by Laufer and the present authors occur near this point.

On the basis of his measurements at Reynolds numbers of 50 000 and 500 000, Laufer concluded that by using the similarity parameters U^* and ν/U^*, the flow field in the region close to the wall becomes independent of the Reynolds number. Comparison of the authors' data for u'_x close to the wall with those of Laufer indicate that his conclusion appears valid at a Reynolds number as low as 5980.

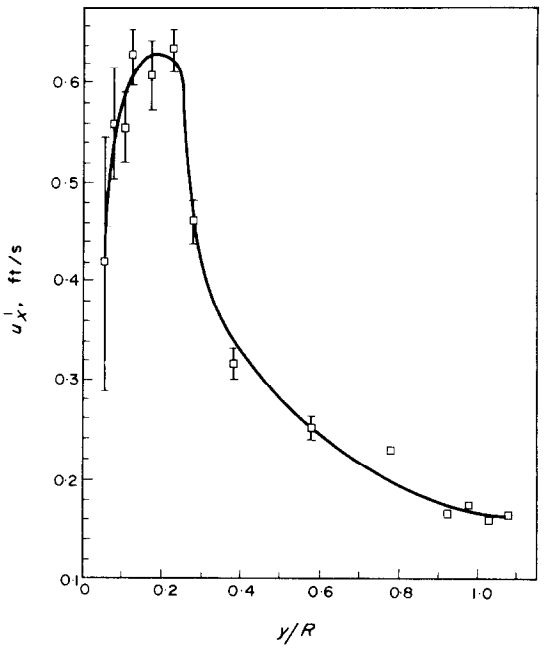

FIG. 10. Nonisothermal turbulent velocity intensities.

The corresponding data for the nonisothermal case (heat flux = 8000 Btu/ft^2 h, Reynolds number = 6032) are given in Figs. 10 and 11. Figure 10 shows the rms axial turbulent intensities u'_x along with the estimated standard errors. In Fig. 11, the same data are plotted using the similarity parameters U^* and ν/U^*,

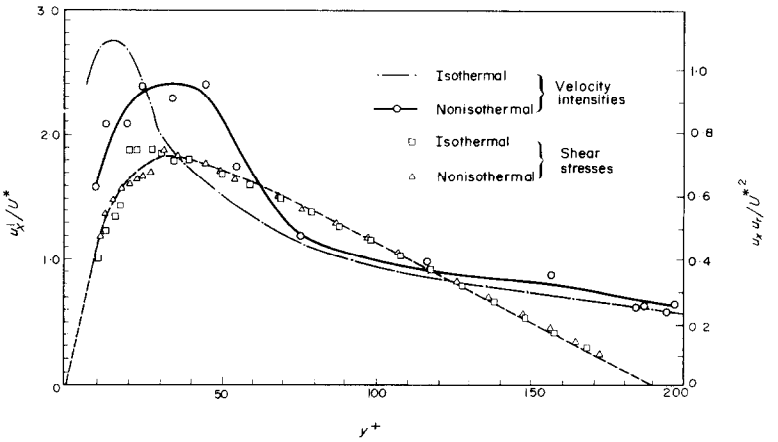

FIG. 11. Turbulent velocity intensities and shear stresses.

together with a dashed curve representing the isothermal data. The radial distribution of the dimensionless turbulent shear stress $\overline{u_x u_r}/U^{*2}$, calculated from the mean velocity profile data is also shown in Fig. 11 as the dotted curve.

As seen from Fig. 11, near the center of the pipe, u'_x/U^* is not affected by the addition of heat flux. Near the wall, however, the u'_x/U^* values for the heat flow condition are much lower than the isothermal values. It should be noted that the Reynolds number based on the bulk fluid temperature was maintained very nearly the same in both conditions, but the true dynamic similarity might not have been maintained.

The distribution of u'_x/U^* reaches a maximum between $y^+ = 25$ and $y^+ = 45$. So does the maximum in the calculated turbulent shear stress.

Temperature fluctuations, t'

Figure 12 shows the radial distribution of rms temperature fluctuations. Between $y/R = 0{\cdot}6$ and $y/R = 1{\cdot}0$, t' changes little with the radial location indicating that the turbulent temperature field is spatially homogeneous in this region.

The magnitude of t' increases as the wall is approached. Since the probe could not penetrate the thermal sublayer, however, its structure could not be investigated.

$\overline{u_x t}$

Figure 13 shows the radial distribution of $\overline{u_x t}$ together with the estimated uncertainty range. The radial distribution of $\overline{u_x t}/U^*T^*$, which is the ratio of the heat flux transported

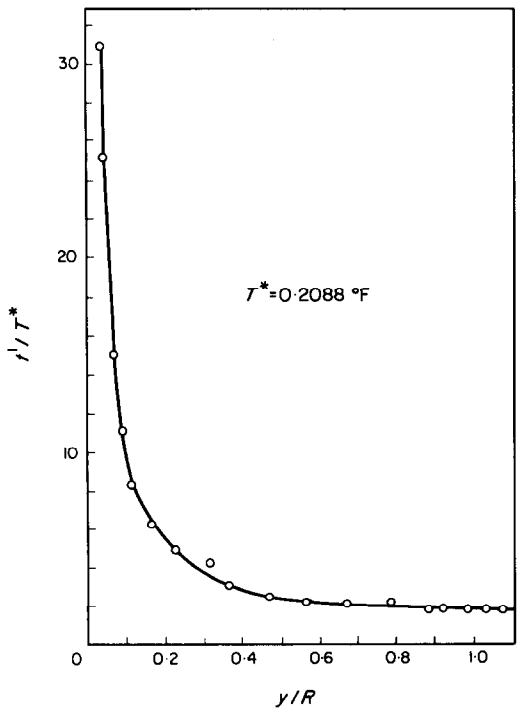

FIG. 12. Temperature fluctuations.

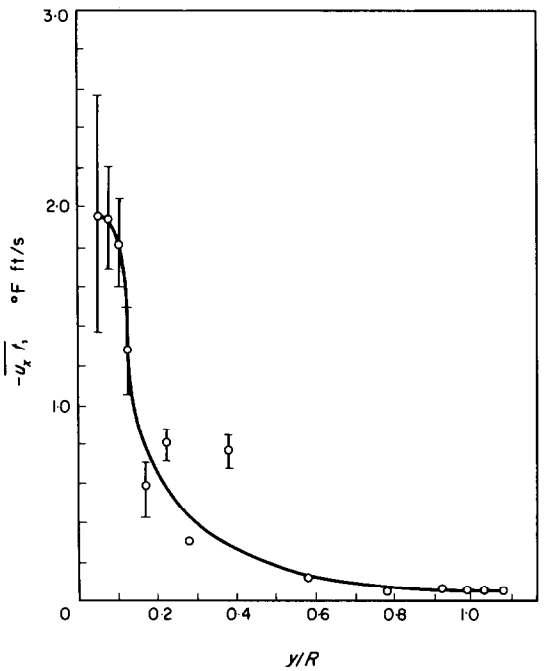

FIG. 13. Turbulent velocity–temperature correlation.

in the axial direction by turbulence to the total flux provided at the wall, is given in Fig. 14. Also shown in Fig. 14 is the distribution of the total radial heat flux transported by molecular conduction and turbulent exchange as a fraction of the total heat flux at the wall.

Since, between $y/R = 0{\cdot}8$ and $y/R = 1{\cdot}0$, the

value of $\overline{u_x t}$ changes little with radial location, the turbulent velocity-temperature field appears to be spatially homogeneous in the radial direction within this region. However, since the values of $\overline{u_x t}$ are very small compared with its maximum value near the wall, the $\overline{u_x t}$ contribution may be considered negligible in this region with the turbulent velocity–temperature field approaching isotropy.

The measured value of $\overline{u_x t}$ at $y/R = 0{\cdot}377$ appears to be inconsistent with the trend of the results and probably should be discarded, although no specific reasons for any unusual errors were noted.

It is seen from Fig. 14 that the axial turbulent heat flux reaches a maximum between $y/R = 0{\cdot}05$ and $0{\cdot}07$ near $y^+ = 10$. At approximately the same location, the total radial heat flux, transported by both molecular diffusion and turbulent exchange, also reaches its maximum value. This behavior is similar to the one shown by u_x' in the absence of heat flux near the edge of the viscous sublayer, as shown in Fig. 11.

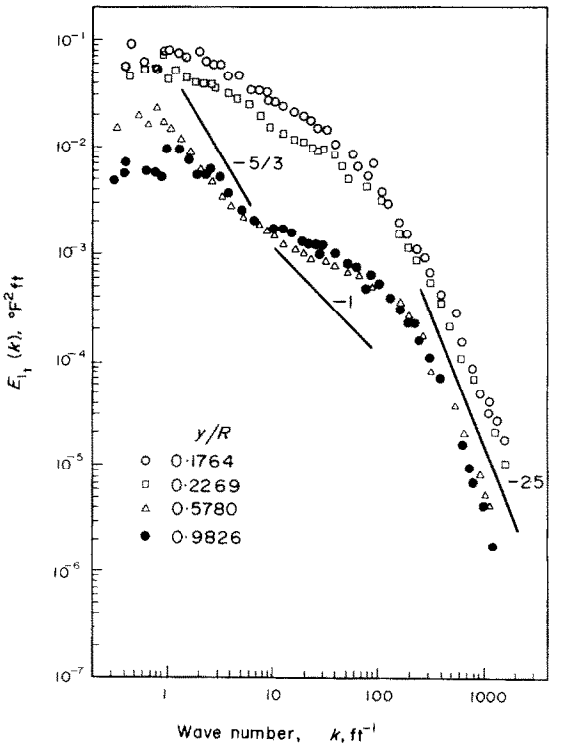

FIG. 15. Temperature fluctuation spectrum.

Temperature spectrum

Figure 15 shows the spectra of temperature fluctuations obtained at locations $y/R = 0{\cdot}176$, $0{\cdot}227$, $0{\cdot}578$ and $0{\cdot}983$. At the last location, at a frequency of 60 Hz the contribution of noise to the total spectrum was comparable to that of the temperature fluctuations. At other frequencies, however, the noise contribution was negligible compared with the signal. The frequency response of the resistance thermometer

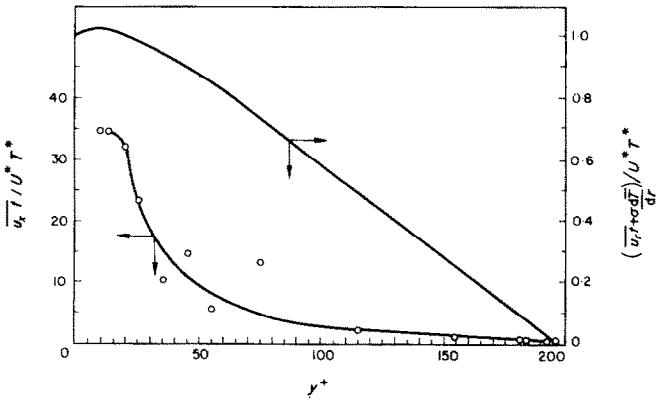

FIG. 14. Radial distribution of heat flux terms.

system limits the interpretation of data to 640 Hz, which corresponds to wave numbers of 800 ft^{-1} at $y/R = 0{\cdot}983$ and 1000 ft^{-1} at $y/R = 0{\cdot}176$.

From Fig. 15, it is seen that the data close to the center of the pipe, at $y/R = 0{\cdot}578$ and 0·983, show two distinct regions before the slope changes to about $-2{\cdot}5$. According to Batchelor's uniform straining model [18] for scalar mixing in high Prandtl number fluids, the spectrum should vary as $k^{-\frac{1}{3}}$ and then follow a k^{-1} dependence. The data for the spectrum of t' near the center of the pipe appear to exhibit a slope of $-\frac{5}{3}$ in a small region of wave numbers, but do not exhibit another region with a slope of -1, as predicted by the model.

At wave numbers above 150 ft^{-1}, the data show a slope of approximately $-2{\cdot}5$ at all locations in the pipe. The temperature spectra in ethylene glycol reported by Rust and Sesonske [9] with a thermocouple sensor at a Reynolds number of 5800 in a pipe also gave a slope of $-2{\cdot}5$ at high frequencies which was independent of location in the pipe.

The velocity spectra

Figure 16 shows the measured one dimensional spectra $E_{1u}(k)$ of the axial velocity fluctuations at six different radial locations, for the isothermal case, as well as the spectrum at $y/R = 0{\cdot}982$ for the non-isothermal case. In computing the latter, the contribution of $\overline{u_x t}$ has been neglected.

From the data shown in Fig. 16, it is seen that a reasonable range of wave numbers in which $E_{1u}(k)$ varies as $k^{-\frac{1}{3}}$ does not exist. At $y/R = 0{\cdot}066$ with $R_\lambda = 432$, there does exist a very small region of wave numbers in which $E_{1u}(k)$ varies as $k^{-\frac{1}{3}}$. From his measurements at $N_{Re} = 50000$ and 500000, Laufer found that for $R_\lambda \gg 200$ and for not too large mean velocity gradients, the spectra of axial velocity fluctuations vary as $k^{-\frac{1}{3}}$, supporting the hypotheses of Kolmogoroff. For the present data, except at $y/R = 0{\cdot}066$ and 0·189, the values of R_λ were less than 200 at all locations (Table 1).

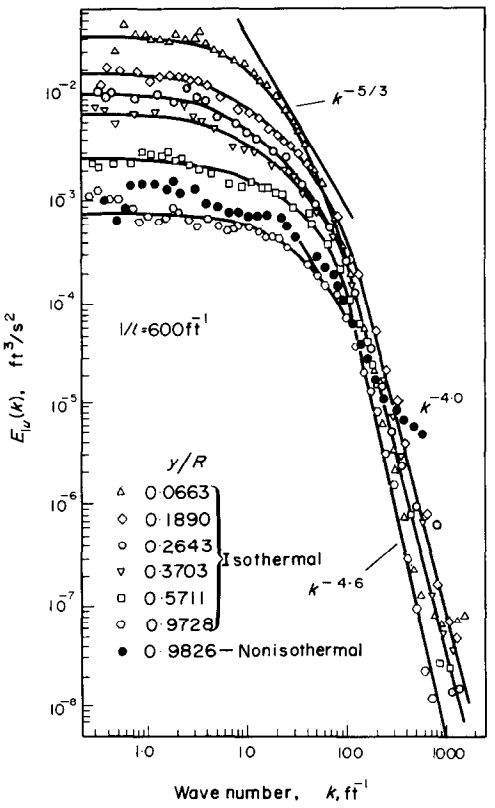

FIG. 16. Velocity fluctuation spectra.

However, since at $y/R = 0{\cdot}066$ and 0·189, the mean velocity gradients were rather high, it is conceivable that the inertial subrange does not exist in the measured spectra.

At high wave numbers, the present data vary as k^{-n} with n having values between 4·0 and 4·6. This is considerably less than the slope of -7 for the energy spectrum at high wave numbers

Table 1. *Isothermal case*, $N_{Re} = 5980$, $q_w = 0$

y/R	λ_x/D	Λ_x/D	R_λ
0·066	0·38	0·73	432
0·189	0·21	1·05	249
0·254	0·20	0·73	127
0·370	0·20	0·61	103
0·571	0·17	0·41	63·5
0·973	0·16	0·33	37·0

predicted by Heisenberg. The mechanism of viscous dissipation at high wave numbers, gives a -4 power dependency on viscosity. On the other hand, the Kolmogoroff theory for the inertial subrange assumes the absence of viscosity effects. If the viscosity dependence of the energy spectrum is assumed so that $E_u(k)$ varies as ν^{-2}, an expression can be obtained for $E_u(k)$ as

$$E_u(k) = \text{const. } \varepsilon_u^a k^b \nu^{-2}. \tag{24}$$

Solving for exponents a and b by dimensional analysis, this reduces to

$$E_u(k) = \text{const. } \varepsilon_u \nu^{-2} k^{-13/3}. \tag{25}$$

The present data at high wave numbers can be qualitatively explained by equation (25). It is interesting to note that for the spectrum of plasma fluctuations at a Reynolds number of 6000, Granatstein *et al.* [26] found three very distinct regions with slopes of $-\frac{5}{3}$, $-\frac{13}{3}$ and -7

By comparing the isothermal spectrum at $y/R = 0{\cdot}973$ with the nonisothermal spectrum at $y/R = 0{\cdot}983$, in Fig. 16, it is seen that near the center of the pipe, below wave numbers of 250 ft^{-1}, the velocity spectrum is not affected by heat flux. Although above this wave number, the estimated spectrum with heat flux flattens considerably, this is regarded as not significant, but a result of errors in the estimation of $E_{1u}(k)$, which involves subtracting two small numbers whose magnitudes decrease with increasing wave number.

Scales of turbulence

The integral scale Λ_x and the microscale λ_x calculated from the spectra of the axial velocity fluctuations for the isothermal case, are presented in Table 1, as fractions of the pipe diameter D. The corresponding values of the turbulent Reynolds number R_λ are also given.

In Table 2 the values of the macroscale Λ_t and the microscale λ_t of the temperature fluctuations estimated at four different radial locations are shown. The microscale and the macroscale of the velocity fluctuations could not be estimated in this case. Therefore λ_x from the isothermal case, at the nearest radial locations has been used for calculating λ_t/λ_x in Table 2.

Table 2. Nonisothermal case.
$N_{Re} = 6032$, $q_w = 8000$ *Btu/h ft²*

y/R	λ_t/D	Λ_t/D	λ_t/λ_x	$1/\sqrt{N_{Pr}}$
0·176	0·057	0·54	0·27	0·1195
0·227	0·049	0·75	0·24	0·1195
0·578	0·056	1·02	0·33	0·1195
0·983	0·055	0·46	0·34	0·1195

It is seen that the macroscales of both velocity and temperature fluctuations are comparable in magnitude to the diameter of the pipe. The microscales of temperature fluctuations are 3 to 4 times smaller than those of velocity fluctuations. In an isotropic turbulent velocity and temperature field, the relation between the microscales of temperature and velocity fluctuations is given by Corrsin as

$$\frac{\lambda_t}{\lambda_x} = \frac{1}{\sqrt{N_{Pr}}}. \tag{26}$$

As seen from Table 2, the predicted values are not in good agreement with the measured ratios.

It should be noted that the ratio of the microscales measured, λ_t/λ_x, is approximately equal to the ratio of the measured thicknesses of the thermal and viscous sublayers, δ_T/δ.

CONCLUSIONS

From the mean velocity profile data at $N_{Re} = 5980$, it was demonstrated that at low Reynolds numbers the mean velocity distribution in the turbulent core lies above the "universal velocity profile." The velocity profile obtained with a wall heat flux of 8000 Btu/h ft^2 agrees with the one obtained under isothermal conditions.

The ratio of the thickness of the thermal sublayer to that of the viscous sublayer was equal to $\frac{1}{4}$, consistent with the relation given

for laminar thermal boundary layers by Eckert and Drake [24] and approximately equal to the ratio of the microscales of the temperature and velocity fluctuations λ_t/λ_x.

Comparison of the present data for u'_x with those of Laufer using the similarity parameters U^* and ν/U^*, indicate that the structure of turbulence within the viscous sublayer seems to be independent of the Reynolds number in the range, $N_{Re} = 5980$–$500\,000$.

The velocity spectra do not indicate the existence of an inertial subrange. At high wave numbers the spectra at all locations vary as k^{-n} with n having values between 4 and 4·6. The velocity spectrum obtained near the center of the pipe for the nonisothermal case indicates that the fine structure of turbulence in that area is not influenced by the heat flux.

Radial distribution of t' and $\overline{u_x t}$ were obtained. The latter quantity has not been previously reported for pipe flow. The values of t', u'_x and $\overline{u_x t}$ reach their maxima near the pipe wall, u'_x between $y^+ = 30$ and $y^+ = 45$; and $\overline{u_x t}$ at $y^+ = 10$. The turbulent shear stress calculated from the mean velocity profile data and u'_x both reach their maximum values at the same location.

Temperature spectra measured at various locations in the pipe do not exhibit two distinct regions of slope $-\frac{5}{3}$ and -1, as predicted by Batchelor's uniform straining model.

ACKNOWLEDGEMENTS

Financial support under National Science Foundation Grant GK-4003 is gratefully acknowledged.

L. E. Hochreiter and R. V. G. Menon provided invaluable assistance in the experimental work and the preparation of the report.

REFERENCES

1. H. C. Reynolds, Jr., Internal low Reynolds number turbulent heat transfer, Ph.D. Thesis, University of Arizona (1968).
2. J. Laufer, The structure of turbulence in fully developed pipe flow, NACATR 1154 (1954).
3. G. K. Patterson, Turbulence measurements in polymer solutions using hot-film anemometry, Ph.D. Thesis, University of Missouri at Rolla, Missouri (1963).
4. J. S. Knox, Pipe flow turbulence, M.S. Thesis, The Ohio State University, Columbus, Ohio (1966).
5. H. P. Bakewell, An experimental investigation of the viscous sublayer in turbulent pipe flow, Ph.D. Thesis. Pennsylvania State University (1966).
6. S. Tanimoto and T. J. Hanratty, Fluid temperature fluctuation accompanying turbulent heat transfer in a pipe, *Chem. Engng Sci.* **18**, 307 (1963).
7. V. I. Subbotin, M. Kh. Ibragimov and E. V. Nomofilov, Statistical study of turbulent temperature pulsations in a liquid stream, *High Temp.* **2**, 59 (1964).
8. V. P. Bobkov, Yu. I. Gribanov, M. Kh. Gribanov, E. V. Nomofilov and V. I. Subbotin, Measurement of intensity of temperature pulsations in turbulent flow of mercury in a tube, *High Temp.* **3**, 658 (1965).
9. J. H. Rust and A. Sesonske, Turbulent temperature fluctuations in mercury and ethylene glycol in pipe flow, *Int. J. Heat Mass Transfer* **9**, 215 (1966).
10. D. S. Johnson, Velocity and temperature fluctuation measurements in a turbulent boundary layer downstream of a stepwise discontinuity in wall temperature, *J. Appl. Mech.* **81**, 325 (1959).
11. S. P. S. Arya, Structure of stably stratified turbulent boundary layer, Ph.D. Thesis, Colarado State University (1968).
12. A. N. Kolmogoroff, The local structure of turbulence in incompressible viscous fluid for very large Reynolds numbers, *The Turbulence, Classic Papers on Statistical Theory*, edited by S. K. Friedlander and L. Topper. Interscience Publishers, New York (1961).
13. W. Heisenberg, On the theory of statistical and isotropic turbulence, *Proc. R. Soc. Lond.* **195A**, 402 (1948).
14. Y. H. Pao, Structure of turbulent velocity and scalar fields at large wave numbers, *J. Fluid Mech.* **5**, 497 (1959).
15. R. Kraichnan, The structure of isotropic turbulence at very high Reynolds numbers, *J. Fluid Mech.* **5**, 497 (1959).
16. A. M. Obukhov, *Izv. Akad. Nauk. SSSR. Geor. i Geofiz.* **13**, 469 (1951).
17. S. Corrsin, On the spectrum of isotropic temperature fluctuations in an isotropic turbulence, *J. Appl. Phys.* **22**, 469 (1951).
18. G. K. Batchelor, Small-scale variation of convected quantities like temperature in turbulent fluid, *J. Fluid Mech.* **5**, 113 (1959).
19. M. M. Gibson, Spectra of turbulence in a round jet, *J. Fluid Mech.* **15**, 161 (1963).
20. J. O. Nye and R. S. Brodkey, The scalar spectrum in the viscous convective subrange, *J. Fluid Mech.* **29**, 151 (1967).
21. A. K. Kudva, Structure of turbulent velocity and temperature fields in ethylene glycol pipe flow at low Reynolds numbers, Ph.D. Thesis, Purdue University (1970).
22. C. W. Hurd, K. P. Chesky and A. H. Shapiro, Influence of viscous effects on impact tubes, *J. Appl. Mech.* **20**, 253 (1953).
23. V. C. Patel and M. R. Head, Some observations on skin friction and velocity profiles in fully developed pipe and channel flows, *J. Fluid Mech.* **38**, 181 (1969).
24. E. R. G. Eckert and R. M. Drake, Jr., *Heat and Mass Transfer*. McGraw-Hill, New York (1965).

25. G. K. PATTERSON and J. L. ZAKIN, Hot film anemometry measurements of turbulence in pipe flow: organic solvents, *A.I.Ch.E. Jl* **13**, 513 (1967).

26. V. L. GRANATSTEIN, S. J. BUCHSBAUM and D. S. BUGNOLO, *Phys. Rev. Lett.* **16**, 504 (1966).

STRUCTURE DES CHAMPS DE VITESSE TURBULENTE ET DE TEMPÉRATURE POUR UN ÉCOULEMENT D'ÉTHYLÈNE-GLYCOL DANS UN TUYAU AU FAIBLE NOMBRE DE REYNOLDS

Résumé—Des profils de vitesse moyenne et des intensités de turbulence ont été mesurés sous des conditions isothermes pour de l'éthylène-glycol s'écoulant à travers un tube vertical de 35,85 mm de diamètre intérieur et pour un nombre de Reynolds de l'ordre de 6000. De plus la moyenne quadratique des fluctuations de température t' et la corrélation $\overline{u_x t}$ entre la vitesse et la température ont été mesurées sous un flux thermique uniforme de 254 kW.m^{-2}, en utilisant une sonde à film chaud. On a déterminé les spectres de température pour différentes positions radiales, le spectre de vitesse au centre du tuyau, et diverses échelles de turbulence.

Les résultats montrent que la distribution de vitesse moyenne dans le moyau turbulent se place au-dessus du "profil universel de vitesse". Une comparaison avec les résultats de Laufer indique que la structure de la turbulence isotherme à l'intérieur de la sous-couche visqueuse est indépendante du nombre de Reynolds dans le domaine $NR_e = 6000$–50000. Près du centre du tuyau U_x' et t' montrent une homogénéité radiale. Dans cette région, le champ de vitesse turbulente-température approche l'isotropie. Les spectres de vitesse comme l'a prédit Kolmogoroff, et de même, les spectres de température ne suivent pas les prédictions du modèle de déformation uniforme de Batchelor, sous les conditions d'expérience à N_{Re} faible et N_{Pr} élevé.

STRUKTUR VON TURBULENTEN GESCHWINDIGKEITS-TEMPERATURFELDERN IN EINEM VON ÄTHYLEN-GLYCOL DURCHSTRÖMTEN ROHR BEI NIEDRIGEN REYNOLDSZAHLEN

Zusammenfassung—Mittlere Geschwindigkeitsprofile und Turbulenzgrade wurden unter isothermen Bedingungen in einem von Äthylen-Glycol durchströmten Rohr mit 35·42 mm Innendurchmesser bei Reynoldszahlen von ungefähr 6000 gemessen. Ergänzend dazu wurden auch die Temperaturschwankung t' und die turbulenten Geschwindigkeits-Temperaturbeziehung $\overline{u_x t}$ bei einem gleichbleibenden Wärmestrom von 2·5 W/cm^2 unter Verwendung eines Heissfilmsensors gemessen. Temperaturspektren an verschiedenen radialen Stellen, das Geschwindigkeitsspektrum in der Rohrachse und verschiedene Turbulenzgrade wurden abgeschätzt.

Die Ergebnisse zeigen, dass die mittlere Geschwindigkeitsverteilung im turbulenten Kern über dem "allgemeinen Geschwindigkeitsprofil" liegt. Ein Vergleich mit den Daten von Laufer zeigt, dass die Struktur der isothermen Turbulenz im Innern der viskosen Unterschicht im Bereich $N_{Re} = 6000$–50000 unabhängig von der Reynoldszahl ist. In der Nähe der Rohrachse weisen u_x' und t' eine radiale Homogenität auf. In diesem Bereich nähert sich das turbulente Geschwindigkeits-Temperaturfeld der Isotropie. Die abgeschätzten Geschwindigkeitsspektren weisen nicht den von Kolmogoroff vorausgesagten Wellenzahlen-Bereich mit der Steigung $-\frac{5}{3}$ auf, noch folgen die Temperaturspektren unter den Versuchsbedingungen (niedrige N_{Re} und hohe N_{Pr}) den Voraussagen nach Batchelors gleichförmigem Beanspruchungsmodell.

СТРУКТУРА ПОЛЕЙ ТУРБУЛЕНТНОЙ СКОРОСТИ И ТЕМПЕРАТУРЫ ПРИ ТЕЧЕНИИ ЭТИЛЕНГЛИКОЛЯ В ТРУБЕ ПРИ НИЗКИХ ЗНАЧЕНИЯХ ЧИСЛА РЕЙНОЛЬДСА

Аннотация—Профили средней скорости и интенсивности турбулентности в изотермических условиях измерялись при течении этиленгликоля по вертикальной трубе с внутренним диаметром в 1,434 дюйма, при числе Рейнольдса ревном 6000. Кроме того, измерялись среднеквадратичная флюктуация температуры t' и корреляция турбулентная скорость—температура $u_x t$ при однородном тепловом потоке, равном 8000 Btu/h

ft², используя датчик с нагретой пленкой. Были определены температурные спектры в различных радиальных положениях, спектр скорости в центре трубы и различные масштабы турбулентности.

Результаты показывают, что распределение средней скорости в турбулентном ядре лежит выше «универсального профиля скорости». Сравнение с данными Лауфера показывает, что структура изотермической турбулентности внутри вязкого подслоя не зависит от числа Рейнольдса в диапазоне N_{Re} = 6000–50 000. Вблизи центра трубы u'_x и t' проявляют радиальную гомогенность. В этой области поле турбулентная скорость—температура приближается к изотропии. Найденные спектры скорости не дают области волнового числа с наклоном в—5/3, как предсказывал Колмогоров.